$\tilde{X}^1A_1$, $\tilde{a}^3B_1$, and $\tilde{A}^1B_1$ States of $SiCl_2$: Ab Initio Calculations and Simulation of Emission Spectra

Foo-Tim Chau,*,† De-Chao Wang,† Edmond P. F. Lee,† John M. Dyke,‡ and Daniel K. W. Mok†

Department of Applied Biology and Chemical Technology, The Polytechnic University of Hong Kong, Hung Hom, Kowloon, Hong Kong, and Department of Chemistry, University of Southampton, Highfield, Southampton SO17, 1BJ, United Kingdom

Received: December 29, 1998

A variety of correlated molecular orbital methods and basis sets have been employed to obtain the minimum-energy geometries, harmonic vibrational frequencies, and relative energies of the $\tilde{X}^1A_1$, $\tilde{a}^3B_1$, and $\tilde{A}^1B_1$ states of $SiCl_2$. The ab initio results obtained have been compared with experimental values, where available. It was found that ab initio methods which are based on unrestricted-spin (UHF) wave functions employing spin-unprojected energies, including the QCISD(T) and CCSD(T) methods and the composite methods of G1 and G2, failed to give a reliable $\tilde{A}^1B_1-\tilde{X}^1\tilde{A}_1$ separation, whereas methods using spin-projected energies or the restricted multireference method MR-CISD/6-311G (2df) gave reliable $\tilde{A}-\tilde{X}$ and $\tilde{a}-\tilde{X}$ separations. The $\tilde{A}^1B_1-\tilde{X}^1\tilde{A}_1$ and $\tilde{a}^3B_1-\tilde{X}^1A_1$ emission spectra of $SiCl_2$ were simulated, employing MP2/6-311G (2df) force constants and compared with available experimental spectra. The geometry of the $\tilde{X}$ state was held fixed at the geometry determined by microwave spectroscopy, and the geometries of the $\tilde{a}^3B_1$ and $\tilde{A}^1B_1$ states were adjusted via an iterative Franck−Condon analysis (IFCA) procedure until the simulated spectra matched best with the observed spectra. The IFCA derived geometry for the $\tilde{A}^1B_1$ state is $r(SiCl) = 2.055 \pm 0.008$ Å and $\theta(ClSiCl) = 119.4° \pm 0.4°$. For the $\tilde{a}^3B_1$ state, $r(SiCl) = 2.041 \pm 0.005$ Å, while the (ClSiCl) angle can have a value of either 115.4° or 114.5°, depending on the vibrational assignments of the experimental spectra.

Introduction

The dichlorosilylene molecule, $SiCl_2$ has been studied a number of times by various spectroscopic techniques,[1−10] partly because of its importance in the semiconductor industry, notably in plasma-etching processes.[1,2,11] The geometry of the $\tilde{X}^1A_1$ state of $SiCl_2$ has been derived from electron diffraction,[10] microwave,[6] and laser-induced fluorescence (LIF)[7] spectroscopic studies. Among these experimentally derived geometries for the ground state of $SiCl_2$, the microwave values of $r(SiCl) = 2.0700 \pm 0.0012$ Å and $\theta(ClSiCl) = 101.25° \pm 0.10°$ are the most reliable, with the smallest quoted experimental uncertainties.

However, for the low-lying $\tilde{A}^1B_1$ and $\tilde{a}^3B_1$ states of $SiCl_2$, it seems that no reliable geometrical parameters are available. Suzuki et al.[1] attempted to extract geometrical information of the upper state from their jet-cooled LIF (excitation) and single-vibrational-level (SVL) dispersed (emission) fluorescence spectrum of the $\tilde{A}^1B_1-\tilde{X}^1A_1$ transition by matching the computed Franck−Condon (FC) intensity patterns with the experimental ones.[1] Employing the method of Coon et al.[12] (the parallel mode approximation) in the FC calculations, four sets of geometrical parameters were possible for the $\tilde{A}^1B_1$ state to fit the experimental envelopes. Among them, two sets were selected, based on deductions made from Walsh's rules ($r(SiCl) = 2.03 \pm 0.17$ Å, $\theta(ClSiCl) = 120.8° \pm 0.9°$ and $r(SiCl) = 2.14 \pm 0.17$ Å, $\theta(ClSiCl) = 116.9° \pm 0.9°$). Clearly, the uncertainties in these derived parameters are large and the authors of this work resorted to results of available ab initio calculations (see later text) for comparison, but no conclusion could be made regarding the preferred choice of parameters.

At this point, it is appropriate to point out that the intensity pattern of the photolytic jet-cooled excitation fluorescence spectrum of Suzuki et al.[1] differs significantly from the pyrolytic jet-cooled LIF excitation spectrum of Karolczak and Clouthier.[5] In the spectrum of Suzuki et al.,[1] which shows maximum intensity at 321.7 nm, the relative intensities of the higher energy vibrational components are much weaker than those in the spectrum of Karolczak and Clouthier,[5] which also shows a vibrationally resolved spectrum but which peaks in intensity at lower wavelength, at 317.4 nm. The strongest observed vibrational component in ref 1 was assigned to the $\tilde{A}(0,7,0) \leftarrow \tilde{X}(0,0,0)$ transition, while in ref 5 the strongest peak was observed at higher energy and was probably associated with the $\tilde{A}(0,10,0) \leftarrow \tilde{X}(0,0,0)$ or $\tilde{A}(0,11,0) \leftarrow \tilde{X}(0,0,0)$ transition. The reasons for the differences in the two LIF excitation spectra are not clear. However, the gas-phase UV absorption spectrum of $SiCl_2$[13] shows lower resolution than either of these studies peaks at 317.4 nm in agreement with the LIF spectrum of ref 5, and shows a very similar envelope to that of ref 5. Hence this indicates that the LIF excitation spectrum of ref 5 is a more reliable representation of the absorption spectrum than the LIF spectrum of ref 1. Hence the vibrationally resolved LIF spectrum of ref 5 for the $\tilde{A}^1B_1 \leftarrow \tilde{X}^1A_1$ transition will be used with our Franck−Condon simulations to estimate the $\tilde{A}^1B_1$ geometry.

In addition, it should be noted that the geometrical parameters given in ref 5 by Meijer et al.[7] for the $\tilde{A}^1B_1$ state of $SiCl_2$ were obtained from analysis of the rotationally resolved LIF spectrum of the $\tilde{A}^1B_1(0,6,0)-\tilde{X}^1A_1(0,0,0)$ transition. Therefore, the parameters derived are those for the (0,6,0) level and not those

* To whom correspondence should be addressed.
† The Polytechnic University of Hong Kong.
‡ University of Southampton.

10.1021/jp984801o CCC: $18.00
Published on Web 06/03/1999

of the (0,0,0) level or the equilibrium geometry. Also, to our knowledge no experimentally derived geometric parameters have been published for the first excited state of $SiCl_2$, the $\tilde{a}^3B_1$ state.

Among the reported $\tilde{a}^3B_1-\tilde{X}^1A_1$ emission spectra, those of Du et al.[3] and Sekiya et al.[4] appear to be of the best resolution and they look to be very similar. Nevertheless, the $\tilde{a}^3B_1-\tilde{X}^1A_1$ T_0 position is uncertain, because of overlapping contributions from excited vibrational levels of the upper state. The assignments of the vibrational components in the observed main $\tilde{a}^3B_1(0,0,0)-\tilde{X}^1A_1(0,\upsilon_2'',0)$ progression given in these two studies differ by one vibrational quantum number in υ_2''. In addition, it appears that the assignments of the next most intense progression are also different, with Du et al.[3] assigning it to the $\tilde{a}^3B_1(0,0,0)-\tilde{X}^1A_1(1,\upsilon_2'',0)$ progression, while Sekiya et al.[4] assign it to the $\tilde{a}^3B_1(0,3,0)-\tilde{X}^1A_1(0,\upsilon_2'',0)$ progression. Reliable spectral simulation would almost certainly help in resolving the above uncertainties. A number of ab initio molecular orbital studies have been reported on the $\tilde{X}^1A_1$, $\tilde{a}^3B_1$, and $\tilde{A}^1B_1$ states of $SiCl_2$.[14−21] However, these calculations, particularly those which calculated minimum-energy geometries and harmonic vibrational frequencies, were performed at relatively low levels of theory (HF/MP2) with a small basis set (6-31G* or DZP). MRCI calculations of the $\tilde{A}^1B_1$ state, which gave geometrical parameters of $r = 2.096$ Å and $\theta(\mathrm{ClSiCl}) = 119.3°$, were mentioned in ref 1, but the details of the calculation and the basis set used seem not to have been published.[21] In the present study, we propose to perform a thorough ab initio study on the $\tilde{X}^1A_1$, $\tilde{a}^3B_1$, and $\tilde{A}^1B_1$ states of $SiCl_2$, employing various types of computational methods and basis sets with the aim of deriving the geometrical parameters of the $\tilde{a}^3B_1$ and $\tilde{A}^1B_1$ states of $SiCl_2$ by simulating their emission spectra, utilizing the experimentally established equilibrium geometry of the $\tilde{X}^1A_1$ state and the computed changes in geometry on excitation to the $\tilde{a}^3B_1$ and $\tilde{A}^1B_1$ states.

Computational Details

Ab Initio Calculations. Since the closed-shell singlet ($\tilde{X}^1A_1$), open-shell singlet ($\tilde{A}^1B_1$), and triplet ($\tilde{a}^3B_1$) states were to be investigated, a variety of computational methods (CIS, CASSCF, MP2, B3LYP, CISD, CCSD(T), MR−CISD, G1, and G2) were employed in order to assess the suitability and reliability of these methods in calculating the quantities: minimum-energy geometries, harmonic vibrational frequencies, and electronic transition energies between these states. For the MP2, B3LYP, CCSD(T), G1, and G2 methods, unrestricted-spin wave functions were employed for the open-shell states in the geometry optimization and frequency calculations, though the spin-projected energies at the MP2 level (PUMP2) were used in the evaluation of the transition energies (see also next section). Spin contamination in the UHF wave function is very small for the $\tilde{a}^3B_1$ state ($\langle S^2\rangle = 2.006$). However, spin contamination is rather large for the open-shell singlet $\tilde{A}^1B_1$ state ($\langle S^2\rangle \approx 1.1$). The CIS, CASSCF, CISD, and MR-CISD methods, however, are spin-restricted methods and hence do not suffer from spin contamination.

It is very likely that because Si and Cl are relatively heavy, previous calculations were limited to use of low levels of theory and/or small basis sets. One way to reduce the cost of computation is to reduce the number of electrons and/or basis functions to be considered in the calculation by freezing core electrons. (In practice, the frozen core approximation was used for all correlated calculations reported here, unless otherwise stated.) This can be achieved by employing effective core potentials (ECPs) for heavier elements. Therefore, other than calculations which used standard all-electron basis sets (6-31G*, 6-31+G*, 6-311 + G(2df), and 6-311 + G(3df)), the standard effective core potential, lanl2,[22] was employed with the following augmented uncontracted valence basis sets:

lanl2(5s5p3d)

Si	5s exponents:	3.0, 1.0, 0.3333, 0.1111, 0.03704
	5p exponents:	2.6365, 0.8505, 0.2744, 0.0885, 0.02855
	3d exponents:	1.925, 0.5, 0.1429
Cl	5s exponents:	4.4037, 1.4679, 0.4893, 0.1631, 0.05437
	5p exponents:	6.5, 2.0313, 0.6348, 0.19836, 0.0627
	3d exponents:	3.5, 1.0, 0.2857

lanl2(5s5p3d1f)

Si: as above + f exponent: 0.35

Cl: as above + f exponent: 0.6

The CIS, CASSCF, MP2, B3LYP, and CCSD(T) geometry optimization and frequency calculations were carried out with the GAUSSIAN 94 suite of programs.[23] In the CASSCF calculations, four electrons and four molecular orbitals were active, i.e., CASSCF, (4,4) and the second root of the CI problem was requested in order to obtain the $\tilde{A}^1B_1$ state. In addition to these calculations, single-point CISD and MR-CISD calculations were carried out with the 6-311G (2df) basis set for the three states considered at their respective MP2/6-311+G-(2df) optimized geometries, employing the GAMESS-UK (6.0) suite of programs.[24] (It should be noted that 6- and 10-component Cartesian d and f functions were used in these GAMESS-UK calculations.) For the CISD calculations, all electrons and molecular orbitals (MOS) were included. For the MR-CISD calculations, in order for the configurational space to be within a manageable size, it was necessary to keep the lowest 15 doubly occupied MOS (corresponding to the $1s^22s^22p^6$ core on each center) frozen and not to include the highest three virtual MOS. The reference configuration set was then increased systematically according to the magnitudes of the computed CI coefficients, until the energy lowering with successive increases in the reference space was less than 0.001 hartree. The largest number of reference configurations used in the MR-CISD calculations for the $\tilde{X}^1A_1$, $\tilde{A}^1B_1$, and $\tilde{a}^3B_1$ states were 22, 16, and 12, respectively, giving corresponding configurational spaces of ca. 4.1, 5.4, and 7.7 million configurations. The Davidson correction[25] was also employed in both the CISD and MR-CISD calculations to estimate the contribution from quadruple excitations (+Q).

Spectral Simulation. The Franck−Condon (FC) simulation method is based on the harmonic oscillator model, including the Duschinksky effect,[26] and has been described elsewhere.[27−30] We have chosen the two $\tilde{A}^1B_1-X^1A_1$ SVL emission spectra of Suzuki et al.[1] (dispersed fluorescence after excitation of the 2_0^5 and 2_1^3 bands) and the $\tilde{a}^3B_1-\tilde{X}^1A_1$ emission spectrum of Du et al.[3] as references against which our simulations will be compared. The geometry of the $\tilde{X}^1A_1$ state was fixed at the microwave experimental geometry of Tanimoto et al.[6] in the iterative FC analysis (IFCA) procedure,[28,29] where the geometric parameters of the upper state were varied systematically (with changes in the parameters initially being given by the results of the ab initio calculations), until the best match between the simulated and observed spectra was achieved. In this IFCA procedure, a Gaussian line shape was used for each vibronic

TABLE 1: Computed and Experiment Geometrical Parameters (r(SiCl) (Å) and θ(ClSiCl) (deg)) and Vibrational Frequencies (in cm^{-1}) of the $\tilde{X}^1A_1$ State of $SiCl_2$

method	r	θ	ν_1	ν_2	ν_3
CASSCF/6-31+G*	2.0828	102.0	532.6	216.1	528.6
MP2/6-31G*	2.0751	101.7	540.8	207.4	539.8
MP2/6-311+G(2df)	2.0767	101.4	530.3	203.7	526.4
B3LYP/6-311+G(3df)	2.0943	101.9	497.9	192.3	488.2
MP2/lanl2(5s5p3d)	2.0599	101.4	521.1	207.0	514.5
CCSD(T)/lanl2(5s5p3d1f)	2.0538	101.7	530.5	206.7	529.1
microwave[a]	2.0700(12)	101.25(10)			
ED/mass[b]	2.083	102.8			
LIF[c]	2.067	101.5		198(3)	
emission[d]				200(2)	
emission[e]			529.2(3.0)	201.2(1.1)	
emission[f]			511(4)	200(2)	
emission[g]				198.5(3.7)	
LIF[h]			521.6(1)	200.6(1)	
IR[i]			512.5	202.2	501.4
IR[j]			513(3)	202(1)	502(3)

[a] Reference 6. [b] Electron diffraction/mass-spectrometry; ref 8. [c] Harmonic values; ref 7. [d] Reference 4. [e] Harmonic values; ref 1. [f] Harmonic values, the average of the two values obtained from two progressions, see ref 3. [g] Reference 2. [h] Harmonic values; ref 5. [i] Reference 8. [j] Reference 9.

TABLE 2: Computed and Experiment Geometries (r(SiCl) (Å) and θ(ClSiCl) (deg)) and Vibrational Frequencies (in cm^{-1}) of the $\tilde{A}^1B_1$ State of $SiCl_2$

method	r	θ	ν_1	ν_2	ν_3
CIS/6-311+G(2df)	2.0613	117.9	474.0	170.4	595.3
CASSCF/6-31+G*	2.0628	119.1	480.5	168.0	611.7
MP2/6-31G*	2.0585	118.6	490.3	164.0	617.0
MP2/6-311+G(2df)	2.0482	118.5	495.0	162.9	626.5
MP2/lanl2(5s5p3d)	2.0297	119.1	492.9	171.5	619.4
CCSD(T)/lanl2(5s5p3d1f)	2.0232	117.4	515.1	162.6	631.2
emission[a]				148.9(3.4)	
emission[b]				149.9(5)	
LIF[c]			428.9(1)	149.75(6)	
IFCA (this work)	2.055(8)	119.4(4)			

[a] Reference 2. [b] Harmonic values; ref 1. [c] Harmonic values; ref 5.

component in the simulations with a full width at half-maximum (fwhm) which was significantly smaller than that in the corresponding observed spectrum. This was necessary in order to assess the changes in the simulated spectral patterns with upper state geometry changes (see next section). The final simulated spectra have, however, employed the appropriate experimental fwhm values.

Results and Discussion

The ab initio results obtained in this work are summarized in Tables 1−4 and compared with available experimental values (the experimental errors, which were quoted in the original papers, are given in parentheses in these tables). The simulated spectra which match best with the experimental spectra are given in Figures 1−6.

Ab Initio Calculations. *Minimum-Energy Geometries.* Considering the optimized geometries of the three states studied, it can be seen that the variation in the computed bond angle, θ, with level of theory and basis sets used is small (within 2°, see Tables 1, 2, and 3) for all states of $SiCl_2$ (except for the $\tilde{a}^3B_1$ state at the CIS level, a level of theory which does not account for electron correlation; see Table 3). The consistency in the computed values of bond angle (θ) suggests that they should be reasonably reliable. Comparing the computed values for the $\tilde{X}^1A_1$ state with the experimentally derived values for this state shows good agreement, supporting this conclusion.

However, the magnitudes of the computed bond lengths, r, at the levels of calculation shown in Tables 1−3, have a rather large spread of ca. 0.04 Å. The calculations with the lanl2-valence-augmented basis sets, lanl2(5s5p3d) and lanl2(5s5p3d1f), gave significantly shorter bond lengths (by ca. 0.02 Å) compared with those from calculations with the all electron basis sets, suggesting that the use of the lanl2-valence-augmented basis sets needs further investigation (see also the later subsection on the computed frequencies and transition energies). Comparing the computed bond lengths with the available experimentally derived values for the $\tilde{X}^1A_1$ state of $SiCl_2$, the B3LYP value is too large, while the MP2 values seem to be the most reasonable (despite the differences between the available experimental values; see Table 1). The basis set effect at the MP2 level on the optimized geometry is very small for the $\tilde{X}^1A_1$ state, though this is not so for the $\tilde{A}^1B_1$ and $\tilde{a}^3B_1$ states. Lastly, it is noted that for the $\tilde{A}^1B_1$ state, although the MRCI bond angle of 119.3° by Kudo et al.,[21] mentioned in the Introduction, agrees well with our computed values, the MRCI bond length of 2.096 Å of ref 21 is considerably larger than all the computed bond lengths in this present work. Since the details of the MRCI calculations of ref 21 are unavailable to us, we are unable to trace the source of this difference.

Vibrational Frequencies. The computed vibrational frequencies obtained at different levels of theory, are quite consistent for the three states studied, including those calculated with the ECP basis sets. The only exceptions are the B3LYP values for the $\tilde{a}^3B_1$ and $\tilde{X}^1A_1$ states which are significantly smaller than the others for all three vibrational modes (Tables 1 and 3). On comparing the computed vibrational frequencies with the experimental values, it should be noted that the computed values given in Tables 1−3 are harmonic values. Harmonic experimental values are also given in these tables where available, and this is stated in the footnote of each table; otherwise, the

TABLE 3: Computed and Experiment Geometries (r(SiCl) (Å) and θ(ClSiCl) (deg)) and Vibrational Frequencies (in cm^{-1}) of the $\tilde{a}^1B_1$ State of $SiCl_2$

method	r	θ	ν_1	ν_2	ν_3
CIS/6-311+G(2df)	2.0474	115.7	524.7	179.6	622.2
CASSCF/6-31+G*	2.0526	117.0	524.2	176.2	633.2
MP2/6-31G*	2.0514	118.2	511.0	168.1	629.7
MP2/6-311+G(2df)	2.0468	117.3	508.8	165.2	622.6
B3LYP/6-311+G(3df)	2.0618	119.2	463.5	153.0	577.3
MP2/lanl2(5s5p3d)	2.0293	117.6	507.0	173.8	616.5
CCSD(T)/lanl2(5s5p3d1f)	2.0265	118.2	504.9	169.7	623.1
emission[a]				159(2)	
emission[b]				164(2)	
IFCA (this work)	2.041(3)	115.4(3)			

[a] Harmonic value: ref 3. [b] Reference 4. [c] See text.

experimental values given are the fundamentals. For the $\tilde{X}^1A_1$ state, where experimental harmonic constants are available for all three modes, the agreement between theory and experiment is quite good, particularly for the ν_2 mode. For the $\tilde{a}^3B_1$ state, experimental values are available only for the ν_2 mode; however, the agreement between theory and experiment is also very good for this mode, particularly for the MP2/6-311+G(2df) computed frequency. For the $\tilde{A}^1B_1$ state, the discrepancies between the computed and observed values are larger than for the other two states. Specifically, the computed values are consistently too large, particularly for the ν_1 mode, though only one experimental harmonic value is available for comparison. Both the CIS and CASSCF values were not in better agreement with experimental values than computer values from other methods, suggesting that the discrepancies are probably not due to the problem of spin contamination associated with the UHF-based correlated methods. In view of the relatively improved agreement with experiment (within ca. 14 cm^{-1}) for the ν_2 frequency at the MP2/6-311+G(2df) and CCSD(T)/lanl2(5s5p3d1f) levels of calculation for this state, it may be concluded that a higher level of theory with better treatment of electron correlation and/or a better quality basis set than has been used would be required to describe the energy surfaces of this open-shell singlet state accurately. However, such calculations would be computationally very demanding. For the purpose of carrying out FC simulations, the MP2/6-311+G(2df) geometries and force constants, which have showed overall good agreement with experiment were employed in this study.

Transition Energies. The computed transition energies given in Table 4 are T_e electronic transition energies, unless stated otherwise in the footnote to the table, while the experimental values are T_0 values. (Using MP2/6-311+G(2df) computed frequencies for the three states shows that the T_e and T_0 values differ by at most 0.003 eV and hence this correction was not made in this work.) For the $\tilde{a}^3B_1-\tilde{X}^1A_1$ transition, if the RHF and CIS values are ignored (because of neglect of electron correlation in these methods), the agreement between theory and experiment is reasonably good. It seems clear that, from the values given in Table 4, the calculations with a large basis set and at a high level of correlation give results which are closer to experiment. The best computed transition energy for the $\tilde{a}^3B_1-\tilde{X}^1A_1$ transition is that at the MR-CISD+Q/6-311G(2df)//MP2/6-311+G(2df) level. The agreement of within 0.05 eV is, indeed, very pleasing. However, it also seems clear that with the achievable accuracy in the computed relative energies at a level of theory/basis attainable with practicable computational means (by taking direct differences of ab initio total electronic energies), it is not yet possible to distinguish between the two assignments of the T_0 position, mentioned in the Introduction, which differ by one vibrational spacing in ν_2'' ($\approx$0.02 eV).

TABLE 4: Computed and Observed Transition Energies (eV) of $SiCl_2$

method	$\tilde{a}^3B_1-\tilde{X}^1A_1$	$\tilde{A}^1B_1-\tilde{X}^1A_1$
RHF/6-311G(2df)	1.55	3.70
CIS/6-311+G(2df)[a]	1.46	3.83
CASSCF/6-31+G*	2.05	4.30
CASSCF/MP2/6-31+G*[b]	1.91	4.84
MP2/6-31G*	2.07	3.64
MP2/6-311+G(2df)	2.18	3.54
B3LYP/6-311+G(3df)	2.29	
MP2/lanl2(5s5p3d)	1.97	3.50
CCSD(T)/lanl2(5s5p3d1f)	2.12	2.46
G1	2.47	2.74
G2	2.42	2.71
CISD/6-311G(2df)[c]	1.99	3.76
CISD+Q/6-311G(2df)[c]	2.15	3.75
MR−CISD/6-311G(2df)[c]	2.18	3.82
MR−CISD+Q/6-311G(2df)[c]	2.31	3.78
experimental[d] (ref 4)	2.32	
experimental (ref 3)	2.36	
experimental (ref 2)		3.76
experimental (ref 1, 5, and 7)		3.72

[a] Vertical transition at the CIS optimized geometry of the corresponding upper states; the rest of the computed values are for the adiabatic transitions at the respective optimized geometries, unless otherwise stated. [b] At the corresponding CASSCF optimized geometries. [c] At the corresponding MP2/6-311+G(2df) optimized geometries. [d] All the experimental values are T_0, while all computed values are T_e, except the G1 and G2 values, which are the enthalpy changes at 298 K.

Nevertheless, attempts were made to investigate this further with the aid of spectral simulation, as will be discussed in the following subsection.

For the $\tilde{A}^1B_1-\tilde{X}^1A_1$ transition, the comparison of experimental and computed transition energies is rather confusing at first sight (see Table 4). In contrast to the $\tilde{a}^3B_1-\tilde{X}^1A_1$ transition, the RHF and CIS transition energies are surprisingly good, while the corresponding CASSCF, CASSCF/MP2//CASSCF, CCSD(T), G1, and G2 values are either too large or too small by over at least 0.5 eV. For the CASSCF and CASSCF/MP2[30] calculations, the poor performance may well be due to the small basis set and small active space employed in these calculations. However, the poor performance of the G1, G2, and CCSD(T) methods is disturbing: the computed transition energies are smaller than the experimental values by $\geq$1.0 eV.

Attempts were made to locate the cause of such poor performance with the G1, G2, and CCSD(T) methods. It was found that the problem was mainly due to the large spin contamination associated with the UHF wave function of the $\tilde{A}^1B_1$ state and the use of spin-unprojected energies for the $\tilde{A}^1B_1$ state in the evaluation of the transition energies. It should be noted that spin contamination does not seem to be a problem for calculating the minimum-energy geometry and harmonic vibrational frequencies for the $\tilde{A}^1B_1$ state as discussed. In addition, it has been reported that the CCSD method usually removes a great deal of the spin contamination.[31] In the case of the open-shell singlet states of BCl_2^+, 1^1B_2, and 1^1A_2, where the spin contamination is of a similar order of magnitude as in the $\tilde{A}^1B_1$ state of $SiCl_2$ reported here, it was found that CCSD(T) transition energies (from the ground state of BCl_2^+) agreed reasonably well with the MRCI values.[32] Nevertheless, for the excitation energy to the $\tilde{A}^1B_1$ state of $SiCl_2$, even the CCSD(T) approach could not rectify the associated spin contamination problem. It should also be noted that the composite methods, G1 and G2, employ both spin-projected (PUMP2) and unprojected {MP4 and QCISD(T)} energies, and hence should be used with caution for calculating the energy of an open-shell singlet state. Finally, it is pleasing that the MR-CISD+Q

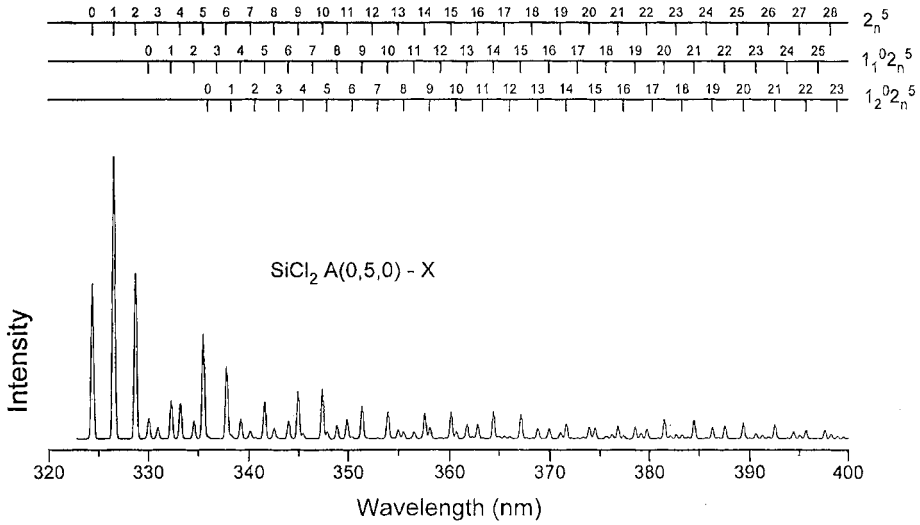

Figure 1. Simulation of the SVL emission spectrum of $SiCl_2$ excited at 325.02 nm (the $\tilde{A}(0,5,0) \leftarrow \tilde{X}(0,0,0)$ excitation). The Gaussian bands used for this simulation have a fwhm of 0.3 nm. This spectrum shows good agreement with the experimental spectrum reported by Suzuki et al. (ref 1, Figure 2). (Reproduced in Figure 7a.)

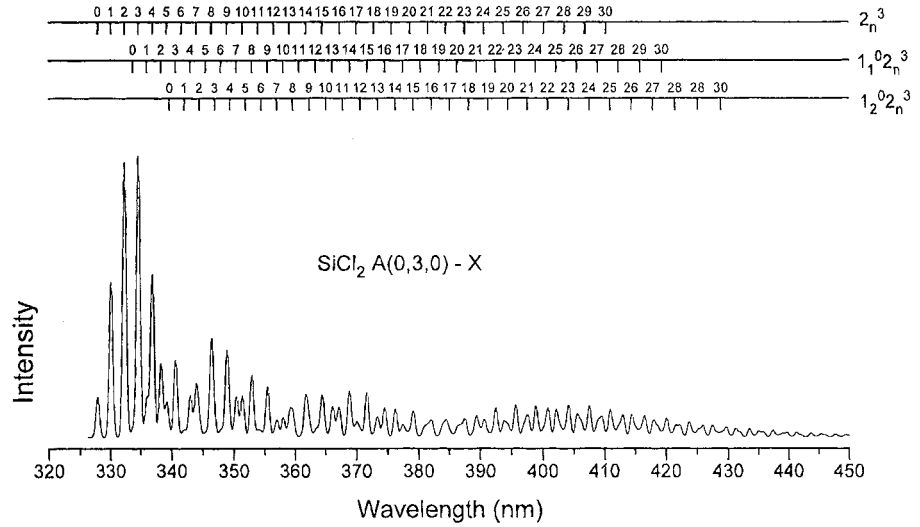

Figure 2. Simulation of the SVL emission spectrum of $SiCl_2$ excited at 330.45 nm (the $\tilde{A}(0,3,0) \leftarrow \tilde{X}(0,1,0)$ excitation). The Gaussian bands used for this simulation have a fwhm of 0.6 nm. This spectrum shows good agreement with the experimental spectrum reported by Suzuki et al. (ref 1, Figure 3). (Reproduced in Figure 7b.)

results agree very well with the experimental values for the $\tilde{A}-\tilde{X}$ transition; similar agreement is obtained for the $\tilde{a}-\tilde{X}$ transition (see Table 4).

Spectral Simulations. *SVL $\tilde{A}^1B_1-\tilde{X}^1A_1$ Emission Spectrum.* The simulated spectra, which match best with the SVL emission spectra of Suzuki et al.,[1] are shown in Figures 1 and 2. Gaussian line shapes with fwhms of 0.3 and 0.6 nm were used to obtain these figures. The IFCA geometry derived for the $\tilde{A}^1B_1$ $SiCl_2$ state, using the procedure described earlier in the Computational Details section, is R(Si−Cl) = 2.055 ± 0.008 Å, and θ(ClSiCl) = 119.4° ± 0.4°.

The rather large uncertainty in the IFCA derived bond length is due to the weak intensities of vibrational components arising from the $\tilde{A}(0,3,0)-\tilde{X}(1,\upsilon_2'',0)$ and $\tilde{A}(0,5,0)-\tilde{X}(1,\upsilon_2'',0)$ progressions in the experimental spectra. The IFCA geometry given above is one which gives the best match for both dispersed fluorescence spectra of $SiCl_2$, excited at 325.02 and 330.45 nm (the $\tilde{A}(0,5,0) \leftarrow \tilde{X}(0,0,0)$ and $\tilde{A}(0,3,0) \leftarrow \tilde{X}(0,1,0)$ excitations, respectively; see ref 1). It should be noted that the observed intensities of the emission peaks at the excitation energies (i.e., the $\tilde{A}(0,5,0) \rightarrow \tilde{X}(0,0,0)$ and $\tilde{A}(0,3,0) \rightarrow \tilde{X}(0,1,0)$ emissions) were enhanced due to contributions from the respective excitation lines. In making the comparison between the simulated and the experimental spectra, these peaks have been ignored. It was found that apart from these peaks, the agreement between the simulated spectra employing the IFCA upper state geometry given above and the experimental SVL spectra is very good. As noted previously,[27,28,33] with the use of the harmonic oscillator model in the FC simulations, it is expected that the agreement between the simulated and experimental spectra would gradually deteriorate for transitions involving high vibrational quantum numbers where the effect of anharmonicity becomes larger. This was found to be the case in Figures 1 and 2 where the agreement for the first 10 resolved components close to the excitation line was good, but the agreement with the features to higher wavelength, which were a lot weaker and not so well resolved, was not so good. The relative intensity of the 10 resolved components close to the excitation line was the structure from which the IFCA upper state geometry was derived.

With $\tilde{A}^1B_1$ IFCA geometry of r(SiCl) = 2.055 ± 0.008 Å and θ(ClSiCl) = 119.4° ± 0.4°, the $\tilde{A}-\tilde{X}$ absorption spectrum

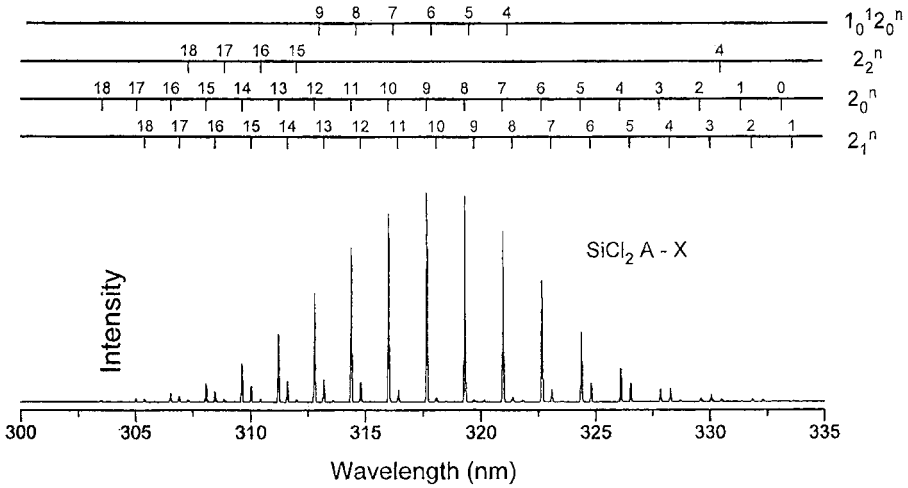

Figure 3. Simulation of the $\tilde{A}-\tilde{X}$ absorption spectrum of $SiCl_2$ using the IFCA derived geometry from Figures 1 and 2 of the $\tilde{A}^1B_1$ state of r(SiCl) = 2.055 ± 0.008 Å and θ(ClSiCl) = 119.4° ± 0.4°. (Reproduced in Figure 7c.) This spectrum was simulated using a Boltzmann distribution of the vibrational levels in the $\tilde{X}^1A_1$ state at a temperature of 150 K. The Gaussian bands in this simulation have a fwhm of 0.02 nm. Good agreement was obtained with the LIF excitation spectrum of ref 5 (see text).

has also been simulated and this is shown in Figure 3. (The simulation was performed using a Gaussian line shape with fwhm of 0.02 nm and at a temperature of 150 K, assuming a Boltzmann distribution of the vibrational levels of the ground state). Although a direct comparison with the LIF excitation spectrum of Karolczak and Clouthier[5] is not possible because of the complex rotational and isotopic structure in ref 5, the simulated envelope agrees well with the experimental envelope, and it is clear that the agreement with the LIF spectrum of Karolczak and Clouthier[5] is much better than with that of Suzuki et al.[1] Given this evidence and the fact that the spectrum of Karolczak and Clouthier[5] shows a similar envelope and maximizes at the same wavelength as the UV absorption spectrum of $SiCl_2$[13] (obtained at lower resolution), unlike the LIF excitation spectrum of Suzuki et al.,[1] we conclude that the LIF fluorescence spectrum of Karolczak and Clouthier[5] is more representative of the absorption spectrum than of Suzuki et al.[1] In addition, the fact that employing the same IFCA geometry in simulating different spectra gave good agreement between theory and experiment in all cases adds weight to the reliability of the method used in extracting geometrical parameters in this way and also to the IFCA $\tilde{A}^1B_1$ geometry thus obtained. It should also be noted that if the geometry of the $\tilde{A}^1B_1(0,6,0)$ $SiCl_2$ state, as determined by LIF spectroscopy,[7] is used in the simulations, very different simulated spectra are obtained for Figures 1, 2, and 3 which are in poor agreement with the corresponding experimental spectra.[1,5]

$\tilde{a}^3B_1-\tilde{X}^1A_1$ Emission Spectrum. The simulated spectrum which matches best with the emission spectrum of Du et al.[3] is shown in Figure 4. A Boltzmann distribution at a temperature of 300 K was assumed for the relative populations of the vibrational levels of the upper state. Variation of the Boltzmann temperature as well as the IFCA geometry was carried out for the simulations. It was found that a temperature of 300 K was adequate to give a simulated intensity pattern which accounts for all the observed transitions arising from excited vibrational levels of the upper state. In addition, the assumption of a Boltzmann distribution seemed adequate. However, the simulations could not account for the underlying unresolved background observed in the experimental spectrum,[3] which also appeared in the observed spectrum of Sekiya et al.[4] Increasing the fwhm of the Gaussian functions used in the simulations even to an extent that some of the observed structure was not resolved still did not reproduce the substantial background in the

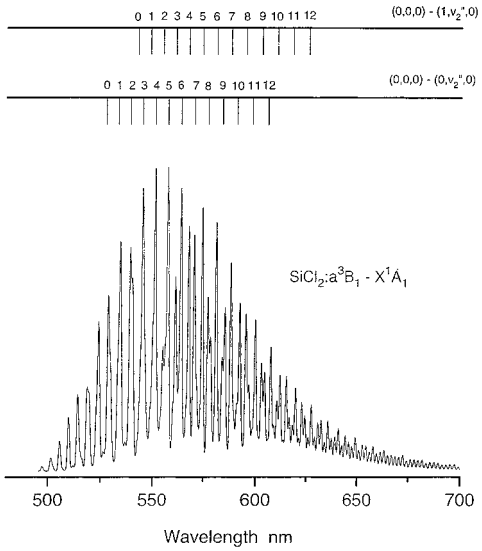

Figure 4. Simulation of the $\tilde{a}^3B_1-\tilde{X}^1A_1$ $SiCl_2$ emission spectrum. This spectrum shows good agreement with that shown in ref 3. The IFCA geometry employed for the $\tilde{a}^3B_1$ state to produce this figure is r(SiCl) = 2.041 ± 0.003 Å and θ(ClSiCl) = 115.4° ± 0.3°. An initial 300 K Boltzmann vibrational distribution in the $\tilde{a}^3B_1$ state was assumed in the simulation.

experimental spectrum. Consequently, the comparison between the simulations and the observed spectrum was based on the resolved fine structure above the background in ref 3 and 4. The IFCA geometry for the $\tilde{a}^3B_1$ state which was used to produce Figure 4 was r(SiCl) = 2.041 ± 0.003 Å, and θ(ClSiCl) = 115.4° ± 0.3°.

It should be noted that in the IFCA procedure, the intensity pattern was found to be very sensitive to upper state geometry variation and this is reflected in the small uncertainties given above for the IFCA geometrical parameters. The absolute uncertainties would be smaller if it were not for the relatively poor resolution of the observed spectrum, and the possibility of an alternative vibrational assignment (see later).

The $\tilde{a}-\tilde{X}$ emission consists of a large number of vibrational series. Figure 5 shows the computed relative intensities of the strongest 10 vibrational series. Based on the vibrational analysis, it is quite certain that the observed second most intense vibrational series is due to the $\tilde{a}^3B_1(0,0,0)-\tilde{X}^1A_1(1,v_2'',0)$

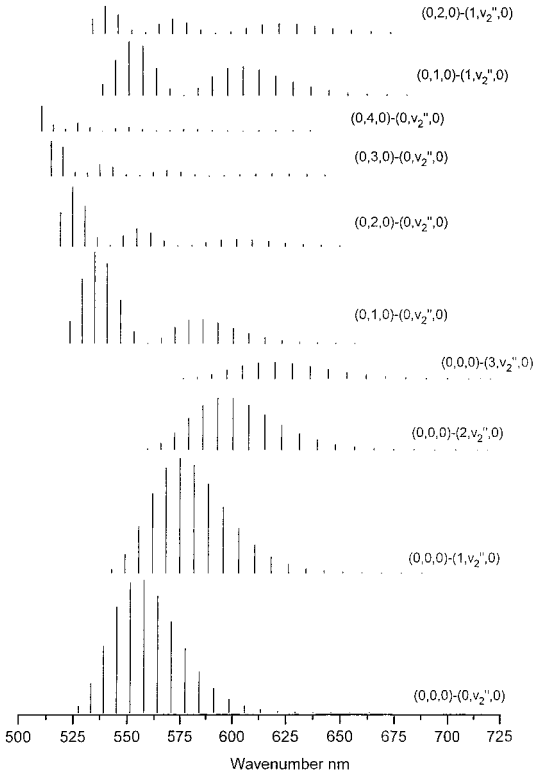

Figure 5. A diagram showing the computed relative intensities of the 10 strongest vibrational progressions in the $\tilde{a}^3B_1-\tilde{X}^1A_1$ emission spectrum. Based on this simulation, it is clear that the observed second most intense vibrational series arises from the $\tilde{a}^3B_1(0,0,0)-\tilde{X}^1A_1(1,\upsilon_2'',0)$ transition as assigned by Du et al.[3] rather than the $\tilde{a}^3B_1(0,3,0)-\tilde{X}^1A_1(0,\upsilon_2'',0)$ transitions assigned by Sekiya et al.[4]

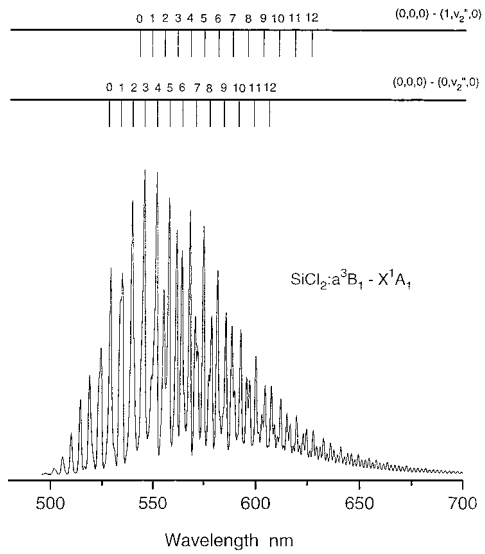

Figure 6. Simulation of the $\tilde{a}^3B_1-\tilde{X}^1A_1$ emission spectra which fits the experimental spectrum with the assignments of Sekiya et al.[4] for the main series (the $\tilde{a}^3B_1(0,0,0)-\tilde{X}^1A_1(0,\upsilon_2'',0)$ series). The best match that was obtained, with the assignment of ref 4, was with an $\tilde{a}^3B_1$ geometry of $r(SiCl) = 2.041 \pm 0.003$ Å, $\theta(ClSiCl) = 114.0° \pm 0.3°$ (see text).

transitions as assigned by Du et al.[3] rather than the $\tilde{a}^3B_1(0,3,0)-\tilde{X}^1A_1(0,\upsilon_2'',0)$ transitions as assigned by Sekiya et al.[4]

Attempts were made to simulate the $\tilde{a}-\tilde{X}$ emission according to the assignments of Sekiya et al.[4] for the main series (the $\tilde{a}^3B_1(0,0,0)-\tilde{X}^1A_1(0,\upsilon_2'',0)$ transitions), so as to determine the position of T_0, as mentioned in the Introduction. The best match is shown in Figure 6. In obtaining this simulated spectrum, the

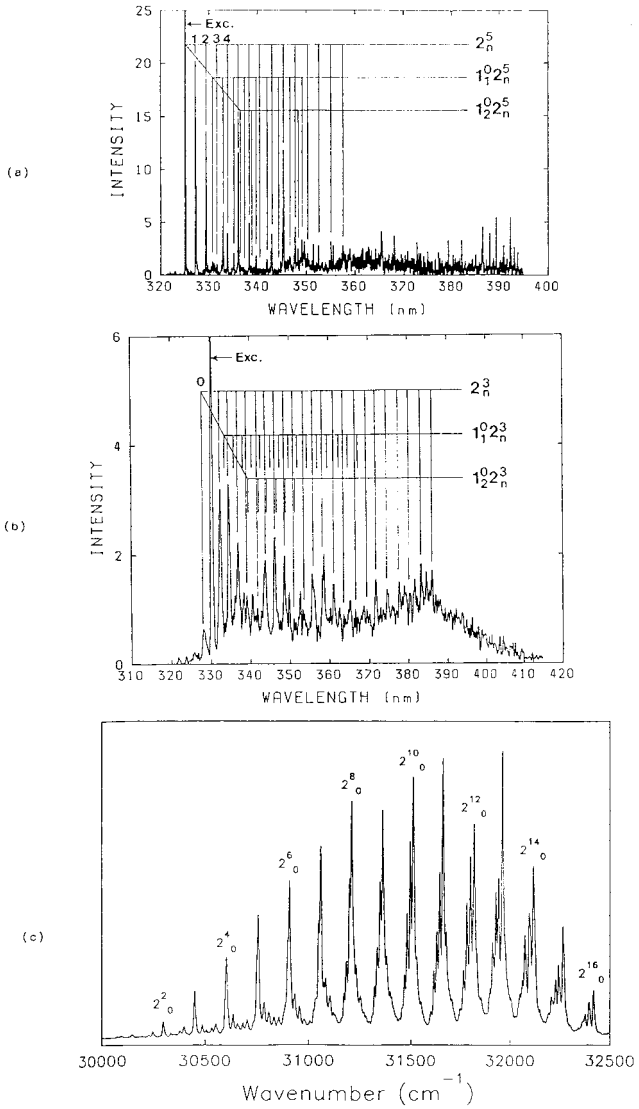

Figure 7. Experimental spectra of $SiCl_2$: (a) Dispersed fluorescence spectrum of jet-cooled $SiCl_2$ recorded on the 2_0^5 excitation. This spectrum can be compared with Figure 1 of the excitation line (marked "Exc") is removed. The spectrum is Figure 2 of ref 1. (b) Dispersed fluorescence spectrum of $SiCl_2$ recorded on 2_1^3 excitation in an effusive flow source. This spectrum can be compared with Figure 2 if the excitation line (marked "Exc") is removed. This spectrum is Figure 3 of ref 1. (c) Experimental $\tilde{A}-\tilde{X}$ absorption spectrum of $SiCl_2$ presented in ref 5, Figure 1. The spectrum was obtained under jet-cooled conditions. Parts a, b (ref 1) and c (ref 2) are reproduced with permission. Copyright 1986, 1993 Elsevier.

IFCA bond angle used was 114.0°, 1.4° smaller than that of the assignment of Du et al.,[3] but the bond length was almost the same as that given above. It can be seen that with a slightly different upper state IFCA geometry, a simulated spectrum similar to that which matches the assignment of Du et al.[3] can be obtained. Comparing the simulated spectra in Figures 4 and 6 with the experimental spectrum of Du et al.[3] in detail, Figure 4 was considered to be a marginally better match, particularly at the low-wavelength region, than Figure 6.

Concluding Remarks

In this work, attempts were made to extract the equilibrium geometries of the $\tilde{a}^3B_1$ and $\tilde{A}^1B_1$ states of $SiCl_2$ from the $\tilde{a}-\tilde{X}$ and $\tilde{A}-\tilde{X}$ emission spectra by spectral simulation using geometries derived from ab initio calculations. It is shown that accurate calculations of the geometries of the low-lying

electronic states of $SiCl_2$ (particularly the bond length) are at present beyond the reach of practical ab initio calculations at reasonably high levels of theory. However, combining such ab initio calculations with FC analysis and spectral simulation, reasonably reliable geometries were obtained and they are probably the most reliable ones currently available for the $\tilde{a}^3B_1$, and $\tilde{A}^1B_1$ states of $SiCl_2$.

Attempts were also made to clarify some disagreements in the assignments of the $\tilde{a}-\tilde{X}$ emission spectra available in the literature. With the spectral simulations provided in this study, the assignment of the observed second main vibrational series should be unambiguous and it is assigned to the $\tilde{A}(0,0,0)-\tilde{X}(1,v_2'',0)$ series. Regarding the $\tilde{a}-\tilde{X}$ T_0 position, it is clear that for such a system such as $SiCl_2$, practical ab initio calculations are still some way from being able to reach an accuracy which could decide between assignments differing by one vibrational spacing. Although our spectral simulations could not distinguish unambiguously between the two proposed assignments from two previous experimental studies, it seems that the assignment of Du et al.[3] is favored. This places T_0 at 2.36 eV for the $\tilde{a}^3B_1-\tilde{X}^1A_1$ transition.

For the $\tilde{A}-\tilde{X}$ emission, attempts were made to rationalize the difference in the spectral pattern between two experimental LIF excitation spectra reported previously and it was concluded that the excitation spectrum of Karolczak and Clouthier[5] should be more representative of the absorption spectrum.[13] The above conclusions show the advantage of combining ab initio calculations with FC simulations in relation to information extractable from the relative intensities observed in emission spectra.

In conclusion, ab initio molecular orbital calculations combined with Franck−Condon simulations have proved very useful in simulating the absorption and emission spectra of $SiCl_2$ and in deriving excited-state geometrical parameters.

Acknowledgment. The authors are grateful to the Research Grant Council of the Hong Kong Special Administrative Region (Project No. PolyU5156/98P) for financial support. The EPSRC, UK, is also acknowledged for computing resources used in this work.

References and Notes

(1) Suzuki, M.; Washida, N.; Inone, G. *Chem. Phys. Lett.* **1986**, *131*, 24.

(2) Sameith, D.; Monch, J. P.; Tiller, H. J.; Schade, K. *Chem. Phys. Lett*. **1986**, *128*, 438.

(3) Du, K.; Chen, X.; Setser, D. W. *Chem. Phys. Lett*. **1991**, *181*, 344.

(4) Sekiya, H.; Nishimura, Y.; Tsuji, M. *Chem. Phys. Lett*. **1991**, *176*, 477.

(5) Karolczak, J.; Clouthier, D. J. *Chem. Phys. Lett.* **1993**, *201*, 409.

(6) Tanimoto, M.; Takeo, H.; Matsumura, C.; Fujitake, M.; Hirota, E. *J. Chem. Phys*. **1989**, *91*, 2102.

(7) Mejier, G.; Henze, J.; Meerts, W. L.; Ter Meulen, J. J. *J. Mol. Spectrosc*. **1989**, *138*, 251.

(8) Mass, G.; Hauge, R. H.; Margrave, J. L. *Z. Anorg. Allgem. Chem*. **1972**, *392*, 295.

(9) Milligan, D.; Jacox, M. E. *J. Chem. Phys*. **1968**, *49*, 1938.

(10) Hargittai, I.; Schultz, G.; Tremmel, J.; Kagramov, N. O.; Maltsev, A. K.; Nefedov, O. M. *J. Am. Chem. Soc.* **1983**, *105*, 2895.

(11) Hopfe, V.; Mosebach, H.; Erhand, M.; Mayer, M. *J. Mol. Struct*. **1995**, *347*, 331.

(12) Coon, J. B.; De Wames, R. E.; Lloyd, C. M. *J. Mol. Spectrosc*. **1962**, *8*, 285.

(13) Ruzsicska, B. P.; Jodhan, A. A.; Safarik, I.; Strausz, O. P.; Bell, T. N. *Chem. Phys. Lett.* **1985**, *113*, 67.

(14) Ha, T. K.; Nguyen, M. T.; Kerins, M. C.; Fitzpatrick, J. *Chem. Phys*. **1986**, *103*, 243.

(15) Gosavi, R. K.; Strausz, O. P. *Chem. Phys. Lett*. **1996**, *123*, 65.

(16) Gordon, M. S.; Nelson, W. *Organometallics* **1995**, *14*, 1067.

(17) Su, M. D.; Schlegel, H. B. *J. Phys. Chem*. **1993**, *97*, 8732.

(18) Ho, P.; Coltrin, M. E.; Binkley, J. S.; Melius, C. F. *J. Phys. Chem*. **1985**, *89*, 4647.

(19) Shin, S. K.; Goddard, W. A.; Beauchamp, J. L. *J. Phys. Chem*. **1990**, *94*, 6963.

(20) Sicilia, E.; Toscano, M.; Mineva, T.; Russo, N. *Int. J. Quantum Chem*. **1997**, *61*, 571.

(21) Kudo, T.; Nagase, S.; Washida, N. To be published; see ref 1.

(22) Wadt, W. R.; Hay, P. J. *J. Chem. Phys*. **1985**, *82*, 284.

(23) *Gaussian 94*, Revision D4; Frisch, M. F.; Trucks, G. W.; Schegel, H. B.; Gill, P. M. W.; Johnson, B. G.; Robb, M. A.; Cheeseman, J. R.; Keith, T.; Petersson, G. A.; Montgomery, J. A.; Raghavachari, K.; Al-Laham, M. A.; Zakrewski, V. G.; Ortiz, J. V.; Foresman, J. B.; Cioslowski, J.; Stefanov, B. B.; Nanayakkara, A.; Challacombe, M.; Peng, C. Y.; Ayala, P. Y.; Chen, W.; Wong, M. W.; Andres, J. L.; Replogle, E. S.; Gomperts, R.; Martin, R. L.; Fox, D. J.; Binkley, J. S.; Defrees, D. J.; Baker, J.; Stewart, J. P.; Head-Gordon, M.; Gonzalez, C.; Pople, J. A. Gaussian Inc.: Pittsburgh, PA, 1995.

(24) GAMESS-UK is a package of ab initio programs written by M. F. Guest, J. H. van Lenthe, J. Kendrick, K. Schoffel, P. Sherwood, with contributions from R. D. Amos, R. J. Buenker, M. Dupuis, N. C. Handy, I. H. Hillier, P. J. Knowles, V. Bonacic-Koutecky, W. van Niessen, R. J. Harrison, A. P. Rendell, V. R. Saunders, and A. J. Stone. This package is derived from the original GAMESS code due to M. Dupuis, D. Spangler and J. Wendoloski, NRCC Software, Catalog., Vol. 1, Program No. QG01 (GAMESS), 1980.

(25) Langhoff, S. R.; Davidson, E. R. *Int. J. Quantum Chem*. **1974**, *8*, 61.

(26) Duschinsky, F. *Acta Physiochem. URSS* **1937**, *7*, 55.

(27) Lee, E. P. F.; Wang, D. C.; Chau, F. T. *J. Phys. Chem*. **1996**, *100*, 19795.

(28) Chau, F. T.; Lee, E. P. F.; Wang, D. C. *J. Phys. Chem*. **1997**, *A101*, 1374.

(29) Chen, P. In *Unimolecular and Bimolecular Ion-Molecule Reaction Dynamics*; Ng, C. Y., Baer, T., Powis, I., Eds.; J. Wiley: Chichester, UK, 1994.

(30) McDouall, J. J.; Peasley, K.; Robb, M. A. *Chem. Phys. Lett*. **1988**, *148*, 183.

(31) Watts, J. D.; Fanz, J. A.; Bartlett, R. J. *Chem. Phys. Lett*. **1996**, *249*, 496.

(32) Lee, E. P. F.; Warschkow, O.; Wright, T. G. *Chem. Phys. Lett*. **1997**, *277*, 264.

(33) Chau, F. T.; Dyke, J. M.; Lee, E. P. F.; Wang, D. C. *J. Electron Spectrosc. Relat. Phenom.* **1998**, *97*, 33.